THE ASTROPHYSICAL JOURNAL, 549:1212–1220, 2001 March 10

THE ZIGZAG PATH OF BUOYANT MAGNETIC TUBES AND THE GENERATION OF VORTICITY ALONG THEIR PERIPHERY

T. EMONET[1]
High Altitude Observatory, National Center for Atmospheric Research, Boulder, CO 80307-3000; emonet@hao.ucar.edu
F. MORENO-INSERTIS[2]
Instituto de Astrofísica de Canarias, E38200 La Laguna, Spain; fmi@ll.iac.es
AND
M. P. RAST
High Altitude Observatory, National Center for Atmospheric Research, Boulder, CO 80307-3000; mprast@hao.ucar.edu
Received 1999 September 10; accepted 2000 October 20

ABSTRACT

We study the generation of vorticity in the magnetic boundary layer of buoyant magnetic tubes and its consequences for the trajectory of magnetic structures rising in the solar convection zone. When the Reynolds number is well above 1, the wake trailing the tube sheds vortex rolls, producing a von Kármán vortex street, similar to the case of flows around rigid cylinders. The shedding of a vortex roll causes an imbalance of vorticity in the tube. The ensuing vortex force excites a transverse oscillation of the flux tube as a whole so that it follows a zigzag upward path instead of rising along a straight vertical line. In this paper, the physics of vorticity generation in the boundary layer is discussed and scaling laws for the relevant terms are presented. We then solve the two-dimensional magnetohydrodynamic equations numerically, measure the vorticity production, and show the formation of a vortex street and the consequent sinusoidal path of the magnetic flux tube. For high values of the plasma beta, the trajectory of the tubes is found to be independent of β but varying with the Reynolds number. The Strouhal number, which measures the frequency of vortex shedding, shows in our rising tubes only a weak dependence with the Reynolds numbers, a result also obtained in the rigid-tube laboratory experiments. In fact, the actual values measured in the latter are also close to those of our numerical calculations. As the Reynolds numbers are increased, the amplitude of the lift force grows and the trajectory becomes increasingly complicated. It is shown how a simple analytical equation (which includes buoyancy, drag, and vortex forces) can satisfactorily reproduce the computed trajectories. The different regimes of rise can be best understood in terms of a dimensionless parameter, χ, which measures the importance of the vortex force as compared with the buoyancy and drag forces. For $\chi^2 \ll 1$, the rise is drag dominated and the trajectory is mainly vertical with a small lateral oscillation superposed. When χ becomes larger than 1, there is a transition toward a drag-free regime and epicycles are added to the trajectory.

Subject headings: hydrodynamics — MHD — Sun: interior — Sun: magnetic fields

1. INTRODUCTION

The motion of magnetic flux tubes in astrophysical media is a complex phenomenon in which the full two- or three-dimensional magnetohydrodynamic structure of the tube plays an important role. Much attention has been devoted to the dynamics of the tubes as one-dimensional deformable ropes with little consideration of the physics of the boundary layer at their periphery or of the surrounding external flows (for a summary, see Moreno-Insertis 1997a, 1997b). Yet, the generation of vorticity in the boundary layer has the potential to modify the trajectory as well as the structure of the flux tube. As with high Reynolds number flows around rigid cylinders in the laboratory, the vorticity generated in the periphery of the tube accumulates in a trailing wake, yielding a von Kármán vortex street. Shedding of oppositely signed vorticity leads to an imbalance of the total vorticity of the tube, the appearance of alternating aerodynamic lift forces, and a consequent sideways deflection of the upward motion (Fan, Zweibel, & Lantz 1998a). The rise of the tube is thus accompanied by a lateral oscillation, yielding a zigzag path.

Vorticity is generated in the magnetic flux-tube periphery essentially through the curl of the Lorentz force, with the buoyancy force being of secondary importance as a vorticity source there (Emonet & Moreno-Insertis 1998). As with the kinetic energy of the flow, viscosity tends to dissipate the vorticity. However, for buoyant magnetic tubes in a stratified medium, the ratio of viscous dissipation to magnetic generation of vorticity, both in the boundary layer, scales as $(R/H_p)(\mathrm{Re}_m/\mathrm{Re})$ (see § 2), where Re and Re_m are the viscous and magnetic Reynolds numbers, respectively, R is the tube radius, and H_p is the local pressure scale height. Whenever $R/H_p \ll 1$ and $\mathrm{Re}_m \lesssim \mathrm{Re}$ (both conditions apply for magnetic tubes in stellar interiors), the magnetic term is predominant and governs the vorticity budget and the formation of the trailing wake.

This paper presents the results of an analytical and numerical study of the generation of vorticity in the boundary layer surrounding a magnetic flux tube and discusses its

[1] Current address: Department of Astronomy and Astrophysics, University of Chicago, 5640 South Ellis Avenue, Chicago, IL 60637; emonet@flash.uchicago.edu.
[2] Also at Departamento de Astrofísica, Universidad de La Laguna, E-38200 La Laguna, Spain.

implications for the buoyant rise of the tube across a stratified medium. We first address the vorticity sources and obtain the basic parameters of the problem and the corresponding scaling laws (§ 2). The magnetic, buoyancy, and viscous terms in the vorticity equation are found to be inversely proportional to the plasma beta. In § 3, we present compelling empirical support for this β^{-1} scaling from 2.5-dimensional numerical simulations of both rectilinear and zigzag rises. In § 4, we examine the Reynolds number dependences. Despite the complexity of the process, an understanding of the results follows from a simplified equation of the motion for the tube (including buoyancy, aerodynamic drag, and vortex forces). Various regimes of rise can be delineated depending on a parameter χ, which measures the importance of the lift force as compared with the aerodynamic drag and is proportional to the square of the vorticity generated in the boundary layer: for $\chi^2 \ll 1$ the dynamics are drag-dominated, whereas for $\chi^2 \gg 1$ they are drag-free (§ 5). The parameter χ grows with increasing Reynolds numbers. A discussion of these results is presented in § 6.

There are several recent publications concerning the two- and three-dimensional structure of buoyant magnetic tubes (e.g., Moreno-Insertis & Emonet 1996; Emonet & Moreno-Insertis 1998; Fan et al. 1998a, 1998b; Hughes & Falle 1998). Their basic astrophysical motivation is to understand the transport of magnetic flux from the interior to the surface of cool stars. Fan et al. (1998a) already noted the detachment of vortex rolls and the ensuing imbalance of vorticity as causing the tube to rise following a zigzag path. In their calculation, however, the vortex loss did not result from a simple instability of the wake but, rather, was directly linked to the presence of a neighboring flux tube. Also related to this paper is a Letter by Hughes & Falle (1998), in which they present the results of a 2.5-dimensional numerical simulation of a rising flux tube at Reynolds number $\sim 10^3$ and $\beta = 10$. The rise of their tube shows a trajectory deviating from the vertical soon after the beginning of the rise. In addition, the tube subsequently stops moving upward and, for a short while, even descends before resuming its rise. In this paper, we argue that these motions are just part of an incipient zigzag oscillation in an intermediate-drag regime, in which the zigzag and the inertial oscillations of a buoyantly accelerated object subjected to a transverse lift force are superposed. In fact, the reversal of the direction of motion just constitutes an *epicycle* typical of this regime of motion: the trajectories found by Hughes & Falle (1998) can be reproduced with our simple analytical model (see Fig. 6 in § 5.3).

2. VORTICITY GENERATION IN THE BOUNDARY LAYER

2.1. *Vorticity Sources*

Consider a plane-parallel stratified medium with equilibrium pressure $p_0(z)$ and density $\rho_0(z)$. A magnetic field distribution in the form of a horizontal magnetic tube is introduced, so that the pressure and density now become $p(x, z) = p_0(z) + \Delta p(x, z)$ and $\rho(x, z) = \rho_0(z) + \Delta\rho(x, z)$, respectively. The main axis of the tube points in the y-direction and the problem is assumed to be 2.5-dimensional: all quantities are invariant in y but vectors may have a y-component. The magnetic field lines may be twisted, and we denote with $\boldsymbol{B}_y$ and $\boldsymbol{B}_t$ the longitudinal and transverse components of the field, respectively. The quantity of interest is the longitudinal vorticity $\omega_y \boldsymbol{e}_y$. Its time evolution is governed by the following equation (Emonet & Moreno-Insertis 1998):

$$\rho \frac{D}{Dt}\left(\frac{\omega_y \boldsymbol{e}_y}{\rho}\right) = \overbrace{\nabla_t\left(\frac{\Delta\rho}{\rho}\right) \times \boldsymbol{g}}^{T_1} + \overbrace{\frac{(\boldsymbol{B}_t \cdot \nabla_t)(J_y \boldsymbol{e}_y)}{c\rho}}^{T_2} + \underbrace{\frac{\mu}{\rho}\nabla^2(\omega_y \boldsymbol{e}_y)}_{T_3} + \underbrace{\nabla_t\left(\frac{1}{\rho}\right) \times \left[-\nabla\Delta p + \frac{\boldsymbol{J} \times \boldsymbol{B}}{c} + \mu\nabla^2 \boldsymbol{u}\right]_t}_{T_4}. \quad (1)$$

The subscript t stands for the component of a vector in the vertical plane, $\boldsymbol{J}$ is the current density, c is the speed of light, and μ is the dynamic viscosity. The effect of compressibility in the viscous term is safely neglected in this equation because the rise velocity is assumed to be much smaller than either the Alfvén (V_A) or the sound (c_s) speed. An asymptotic analysis based on the small parameters β^{-1} and R/H_p (appropriate for buoyant magnetic tubes in the lower solar convection zone where typically $\beta \gtrsim 10^5$ and $R/H_p \lesssim 10^{-2}$) shows that the fourth term on the right-hand side of equation (1), T_4, is $O(\beta^{-1})$ smaller than the other three, T_1, T_2, and T_3 (Emonet & Moreno-Insertis 1998). These first three terms correspond to vorticity generation by buoyancy (baroclinic production, T_1) and magnetic stresses (T_2), and to the viscous dissipation (T_3), respectively. The viscous term is the only one present in laboratory experiments with flows around rigid cylinders.

If the magnetic field lines are assumed to be sufficiently twisted for the tube to maintain coherence during its rise, but still with $|\boldsymbol{B}_t|$ smaller than $|\boldsymbol{B}_y|$, then within the interior of the tube, the first two vorticity generation terms of equation (1) compete with each other in an oscillatory fashion with time (Moreno-Insertis & Emonet 1996). In the tube boundary layer (where the magnetic field distribution falls to zero), however, they reinforce each other, generating oppositely signed horizontal vorticity on either side of the tube. This vorticity, in fact, has the same sign as that generated around rigid cylinders in high-Re laboratory experiments, which produces the characteristic vortex rolls in the wake.

2.2. *Scaling Laws*

We are interested in high Reynolds number flows for which the width of the boundary layer is much smaller than the radius of the tube. The structure of the boundary layer depends on the ratio $\mathrm{Re}_m/\mathrm{Re}$. If $\eta \ll \nu$, with η the magnetic diffusivity and ν the kinematic viscosity, then there are two boundary layers, with the resistive one being much thinner than the viscous one (e.g., Parker 1982). The situation, in fact, is comparable to what we would get along a rigid cylinder in the sense that vorticity is produced within the very thin resistive layer (the analogy is better in the limit $\mathrm{Re}_m \to \infty$) and diffused into the wider viscous layer where it is transported downstream. In the convection zone, on the other hand, one expects η to be larger than ν; whenever $O(\mathrm{Re}_m) \leq O(\mathrm{Re})$, the tangential velocity should fall to zero over a distance δ equal to the width of the resistive bound-

ary layer, i.e.,

$$\delta \approx R/\sqrt{\mathrm{Re}_m}\ , \tag{2}$$

since the magnetic field exerts a tangential stress on the fluid *everywhere* within the resistive boundary layer. Because of the constraints imposed by the numerics, in this paper Re_m and Re are of the same order of magnitude (η is a factor of 2 to 3 smaller than ν).

Let us call V_{tube} the modulus of the velocity of the tube in the vertical plane. To obtain an estimate for the magnetic vorticity source (T_2) and the sink term (T_3), we consider the asymptotic case in which the drag force exactly balances the driving forces in the equation of motion of the tube, so that the inertial term is negligible (this will be called the *drag-dominated* regime). Setting the buoyancy force equal to the drag force yields for the velocity of the tube the asymptotic equilibrium value V_{eq}, given by

$$V_{\mathrm{tube}} \approx V_{\mathrm{eq}} \equiv \frac{c_s}{\beta^{1/2}} \left(\frac{R}{H_p}\right)^{1/2}\ . \tag{3}$$

With this value, and on the basis of equation (2), we obtain

$$\frac{(\boldsymbol{B}_t \cdot \boldsymbol{\nabla}_t)(J_y \boldsymbol{e}_y)}{c\rho} = O\left[\frac{\mathrm{Re}_m^{1/2}}{\beta}\left(\frac{c_s}{R}\right)^2 \underbrace{\sin^2 \Psi}_{O(1)}\right], \tag{4}$$

$$\frac{\mu}{\rho}\nabla^2(\omega_y \boldsymbol{e}_y) = O\left[\frac{\mathrm{Re}_m^{3/2}}{\mathrm{Re}}\frac{1}{\beta}\left(\frac{c_s}{R}\right)^2\left(\frac{R}{H_p}\right)\right]. \tag{5}$$

Ψ is the pitch angle of the field lines. The use of equation (2) restricts the validity of these estimates to the case $O(\mathrm{Re}_m) \leq O(\mathrm{Re})$ (otherwise the tangential velocity would fall to zero over a distance wider than $R/\mathrm{Re}_m^{1/2}$). The buoyancy source term T_1 in equation (1) obeys a scaling law similar to (5) but without the dependence on the Reynolds numbers. The main parameters of the problem are, therefore, the plasma beta, the tube radius, and the viscous and magnetic Reynolds numbers.

All three terms T_1 through T_3 depend on the plasma beta as β^{-1}. Hence the solutions obtained should show this simple scaling. On the other hand, the asymptotic speed of rise and, therefore, the inverse timescale for each solution scale as $\beta^{-1/2}$. A test for all these scaling laws is contained in the following section, which is devoted to a numerical study of the rise of buoyant tubes for different values of β but maintaining Re and Re_m constant. The dependence on the Reynolds numbers is studied in § 4.

For an actual tube in a stellar interior, Re (or Re_m) and β are not independent parameters: the speed of rise depends on β, so that Re and $\mathrm{Re}_m \propto V_{\mathrm{tube}} \propto \beta^{-1/2}$. The separation of dependences used in the following sections is just a device that facilitates the numerical test of the scaling laws: while we can vary β within a range of a few orders of magnitude, the current numerical codes do not allow the same for the Reynolds numbers.

3. THE RISE OF BUOYANT MAGNETIC FLUX TUBES FOR VARYING VALUES OF β

The actual trajectory of the buoyant tubes sensitively depends on the nature and instabilities of the trailing wake, which, in turn, results from the generation of vorticity in the boundary layer. This section examines, using numerical simulations, two different types of trajectories, namely, rectilinear (§ 3.1), which applies when the wake does not become unstable, and sinusoidal, after the vortex-shedding instability has already set in (§ 3.2). At the same time, we will be testing the scaling laws discussed just above. To that end, in this section we keep the Reynolds numbers fixed and use different values of the plasma beta.

We use an explicit code that integrates the complete set of compressible MHD equations in two dimensions, including viscosity, magnetic diffusion, and thermal conduction. No special artificial viscosity is implemented. The code is a modification of a hydrodynamic code used to simulate the dynamics and stability of compressible plumes (Rast 1998). The background atmosphere is adiabatically stratified, with pressure and density ratios across the box of 6 and 3, respectively. The initial tube is given by $B_y \sim \exp(-2r^2/R^2)$, $\boldsymbol{B}_t = q\boldsymbol{r} \times \boldsymbol{B}_y$, with $\boldsymbol{r}$ drawn from the tube center, $qH_p = 10.5$, and $R/H_p = 5.7 \times 10^{-2}$.

3.1. *Rectilinear Trajectories*

We have run simulations for initial values of β at the tube center equal to 800, 400, 200, 100, 50, and 25. The viscosity and ohmic diffusivity are adjusted (in factors of 2) for each run so that the resulting viscous and magnetic Reynolds numbers of the solutions are approximately equal. Calculating Re and Re_m based on the horizontal width of the tube and its rise velocity, values during the asymptotic rise regime fall between 200 and 300 for Re and between 700 and 800 for Re_m. All other parameters are kept fixed. For these values of β, Re, and Re_m, the wake is stable during the rise across the integration box and the resulting trajectory of the tube is a simple straight line (as in, e.g., Emonet & Moreno-Insertis 1998).

To test the scaling laws of § 2.2, we plot in Figure 1 the time evolution of the *positive* vorticity integrated over the right half of the tube wake. The region of integration is a square spanning horizontally the right half of the box and extending vertically all the way up to the stagnation point at the rear of the tube. The unit of time is the same for all curves and is taken as $H_p/(V_{\mathrm{A}})_{\beta=25}$ (V_{A} is the Alfvén speed at the center of the tube at $t = 0$ and the subscript $_{\beta=25}$ means that V_{A} for the case with $\beta = 25$ is used). Except during the initial stages of evolution, when the asymptotic quasi-equilibrium between buoyant acceleration and aerodynamic drag is being reached, the total amount of positive vorticity in the wake increases linearly with time. At the Reynolds numbers being considered, there is little dissipation of vorticity in the wake over the elapsed time shown. Thus the accumulated *positive* vorticity in the right half of the tube wake is a good indicator of its rate of generation in the right magnetic boundary layer. If we now rescale each curve using H_p/V_{A} (which is proportional to $\beta^{1/2}$ and equal to each curve's own timescale) and plot them again, we obtain the curves of the lower panel. As can be seen, the curves now overlap in the asymptotic quasi-equilibrium regime. This clearly shows how well the scaling law of the previous section applies. The quality of the result stems mainly from the fact that both the generation and dissipation terms depend on β^{-1}. It also follows from the exclusion from the measurement of the *negative* vorticity, produced at the rear of the tube, which would have blurred the results.

3.2. *Vortex Shedding and the Zigzag Trajectory*

If the initial condition is not perfectly symmetric, then for the Reynolds numbers considered here the wake becomes

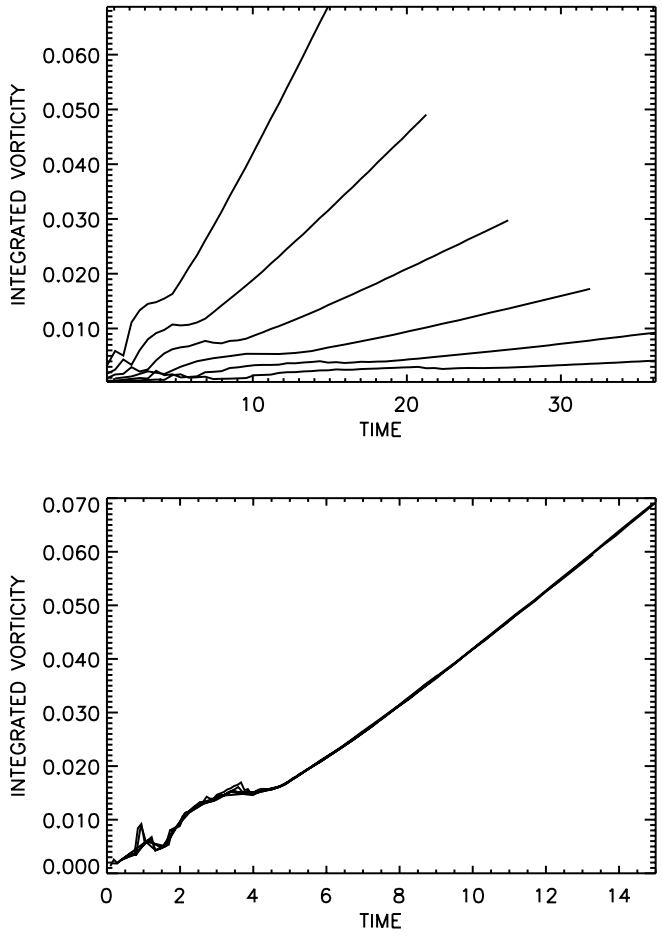

FIG. 1.—*Top:* Amount of positive vorticity on the right-hand side of the wake as a function of time for different values of β. From left to right, the curves correspond to $\beta = 25$, 50, 100, 200, 400, 800. The time unit is $H_p/(V_A)_{\beta=25}$ (which is common to all curves). *Bottom:* Same vorticity values but with a different scaling—both the vorticity and inverse time of each curve have been multiplied by V_A/H_p, i.e., the time unit for each curve is made proportional to $\beta^{-1/2}$. The nice superposition of the curves in the asymptotic regime confirms the β^{-1} law.

unstable, and trailing vortices are shed alternatively from either side of the tube. The detachment of a vortex roll from the wake to the trailing von Kármán street causes a vorticity imbalance, i.e., a nonzero net circulation around the tube and an associated lift force. In this section, we show how this leads to a zigzag rising path of the tube. In the laboratory experiments, the instability takes place whenever $\mathrm{Re} \gtrsim 40$ and is present for a few orders of magnitude above that figure (Williamson 1996). Given the similarities between rigid cylinders and buoyant twisted tubes (Emonet & Moreno-Insertis 1998), we expect the latter to yield a similar dependence of the instability on the Reynolds numbers.

To study the phenomenon of vortex shedding numerically, we have to induce its onset by giving the tube interior an initial nonzero net vorticity. This is because, as shown in the previous subsection, at the Reynolds numbers used in the simulations, the vortex shedding takes too long to start in the numerical experiments. We initiate a series of experiments ($\beta = 50$, 100, 200, and 400) with the same background atmosphere and magnetic field configuration as those described at the beginning of § 3 but with a plateau-like vorticity distribution within the tube and a circular vortex-sheet of the opposite sign surrounding it. In keeping with the scaling laws of §§ 2.2 and 3.1, and using again H_p/V_A as time unit for each curve, we expect the total vorticity to scale as $\beta^{-1/2}$ and thus choose the height of the vorticity plateau to be proportional to $\beta^{-1/2}$ as well: $\omega_0 = 0.8V_A/H_p$. On the other hand, we scale η and ν so that Re and Re_m have the same value in all the calculations.

As illustrated by Figure 2, the initial right-left asymmetry in the external flow relative to the tube produces a strongly asymmetric wake from the beginning. The vortex on the side of maximum shear develops vigorously, while that on the other side remains comparatively small. This causes a vorticity imbalance, so that the tube is pushed sideways as a result of the vortex force acting on it (see, e.g., Saffman 1992). When the main vortex has developed sufficiently, it detaches from the tube and is left behind. The remaining wake, together with the tube, now has excess vorticity of the opposite sign to the original value, and the vortex force pushes them laterally in the opposite direction. The other vortex in the wake grows vigorously and, when the horizontal deflection of the tube is close to its maximum, it too is shed. These are the two first episodes in the formation of the von Kármán vortex street.

The actual trajectories on the x-z plane followed by the four cases with different β are *nearly identical* (see Fig. 3), as are their temporal evolution (see Fig. 5). This is because of the $\beta^{-1/2}$ dependence of speed of rise, inverse timescale of the solutions, and total vorticity generated, which lead to a β^{-1} dependence of all forces acting on the tube (buoyancy, drag, and vortex forces). Thus, changing β *in the range* $\beta \gg 1$ *with constant* Re *and* Re_m *causes a change in the speed of rise but not in the trajectory* followed by the tube, as clearly demonstrated by Figure 3. This result provides further confirmation of the scaling laws derived in § 2.2. The present analysis does not apply if the plasma beta used for the simulation is too small: terms of order 2 and higher in $1/\beta$ must then be retained in equation (1).

The frequency of shedding of vortices has the same scaling $\propto \beta^{-1/2}$ as all other inverse times of the problem. This is a direct consequence of the dependence of the frequency of shedding on the velocity of the tube as V_{tube}, which is a very general result also observed in the case of flows around rigid cylinders in the laboratory. This is explained in the following section.

4. VORTEX SHEDDING FOR VARYING REYNOLDS NUMBERS

In this section, we study the dependence of the trajectory of the magnetic tubes on the Reynolds number: we maintain the value of the plasma beta constant ($\beta = 50$) and carry out five simulations with values of η and ν differing by factors of 2 from experiment to experiment. The corresponding Reynolds numbers range from 50 to 300 (Re) and 100 to 600 (Re_m).

A number of complications appear when analyzing the vorticity in the wake of a rigid cylinder in high-Re ranges. For instance, as explained by Berger & Wille (1972), the net circulation in one rolled-up vortex is diminished by the sweeping of vorticity from one side to the other of the wake, which mixes fluid parcels with opposite signs of vorticity. The importance and consequences of this transport of vorticity depend not only on the diffusivity but also on the geometry of the wake (size of the rolls, etc.), which, in turn,

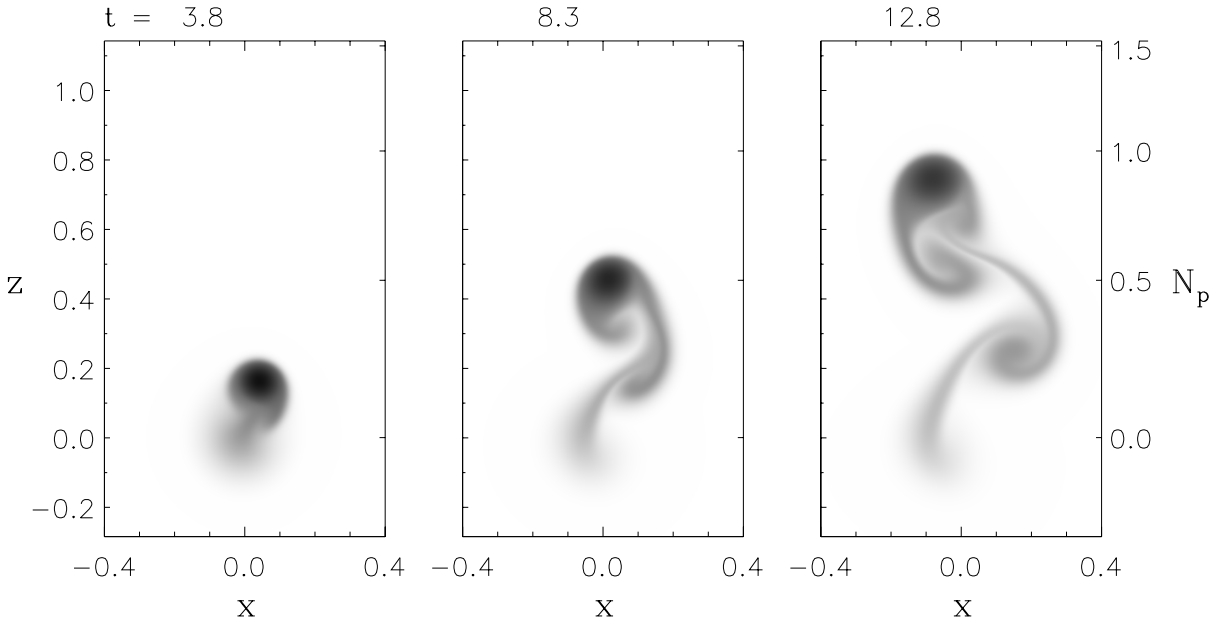

FIG. 2.—Rise of a twisted tube with $\beta = 400$ through a stratified environment. Gray scale represents the intensity of B_y. The initial tube is rotating according to a vorticity plateau with $\omega_0 = 0.8 V_A/H_p$. The first two stages of formation of a von Kármán vortex street are apparent in the figure. They lead to a sideways oscillation of the rising tube.

depends on the Reynolds number in a nontrivial way. In a three-dimensional situation, we know, moreover, that for $\mathrm{Re} > 200$ the wake develops a rich structure (Williamson 1988b, 1996). Despite these difficulties, one can find in the hydrodynamic literature clear results for the measurement of at least two magnitudes relating to vortex shedding behind cylinders: the frequency of shedding of rolls and the amplitude of the associated fluctuations in the lift force. These measurements can serve as a rough guide for the behavior of rising flux tubes with unstable wakes.

From the hydrodynamic literature, we know that the frequency of vortex shedding, f, changes little (in dimensionless terms) over a wide range of Re. This is measured by the Strouhal number, $\mathrm{St} = f D_{\mathrm{tube}}/V_{\mathrm{tube}}$, with D_{tube} being the horizontal size of the tube. In the hydrodynamic measurements, the deviation of St from the mean value is never larger than about 10% for $200 \leq \mathrm{Re} \leq 2 \times 10^5$ (see, e.g., Norberg 1994 and Fig. 4 in this paper). Can we expect a similar behavior for the case of buoyant magnetic tubes as Re_m is increased?

For each of our simulations, we measure the Strouhal number and find values close to the hydrodynamic data. This is shown in Figure 4. The solid line represents the hydrodynamic results on the Strouhal-Reynolds number relationship for vortex shedding of a circular cylinder (see Williamson 1988a, 1988b; Norberg 1994; and Williamson 1996). The circles correspond to our simulations. The error bars account for the latitude in evaluating D_{tube}, V_{tube}, and Re (the speed of rise oscillates around the terminal velocity, the Reynolds number is proportional to the density, etc.). The discrepancy between magnetic tube and hydrodynamic data is less than 20% in all calculated cases except the most diffusive one (which, in any case, is on the border of the Re range for which the definition of St makes sense).

For the range of Reynolds numbers considered in our simulations, the motion is basically vertical with a small horizontal oscillation superposed, so that the vertical speed is not far from the forward speed of the tube, $\mathrm{V}_{\mathrm{tube}}$. The vertical wavelength of the oscillation is thus $\lambda \approx D_{\mathrm{tube}}/\mathrm{St}$. This provides a simple method for measuring St. Moreover, since St does not change too much, as long as $V_{\mathrm{tube}} \approx V_{\mathrm{eq}}$ (see eq. [3]), one should expect the wavelength to be close to that shown in Figure 3 independently of Re or Re_m.

Alongside the vorticity production, the amplitude of the fluctuations in lift force grows with increasing Re_m; experimental data on vortex shedding confirm this for a wide range of Reynolds numbers (see Fig. 5*b* in Szepessy & Bearman 1992). The exact proportionality and power of equations (4) and (5), however, can only hold for not too high Re_m: beyond a threshold in Re_m, V_{tube} does not reach the equilibrium value V_{eq} of equation (3). In fact, when the lift force is dominant, the trajectory of the tube may become quite complicated. All this renders the comparison with the rigid cylinder experiments difficult and blurs the notion of a single frequency of vortex shedding for the flux tube. In § 5, we show through an analytical model how the velocities and trajectories are affected when the lift force becomes important compared with the other forces.

5. THE ZIGZAG PATH AS A CONSEQUENCE OF AERODYNAMIC LIFT, DRAG, AND BUOYANCY

5.1. *Analytical Model*

The trajectory followed by the tubes in Figure 3 can be described approximately using a simple equation of motion for a *vortex filament* subject to the buoyancy and drag forces. Let Ω be the mean value of the y-component of the total vorticity in a vertical cross section, σ, of the tube and the recirculation region, $\Omega = S^{-1} \int_\sigma \omega_y \, dS$, and $\boldsymbol{v}$, the average tube velocity in the vertical plane. An infinitely thin horizontal vortex filament of strength Ω experiences the vortex force $\Omega \boldsymbol{v} \times \boldsymbol{e}_y$ in addition to any other external force acting on it (Saffman 1992). If we add to that the drag and buoyancy forces, the following equation of motion results:

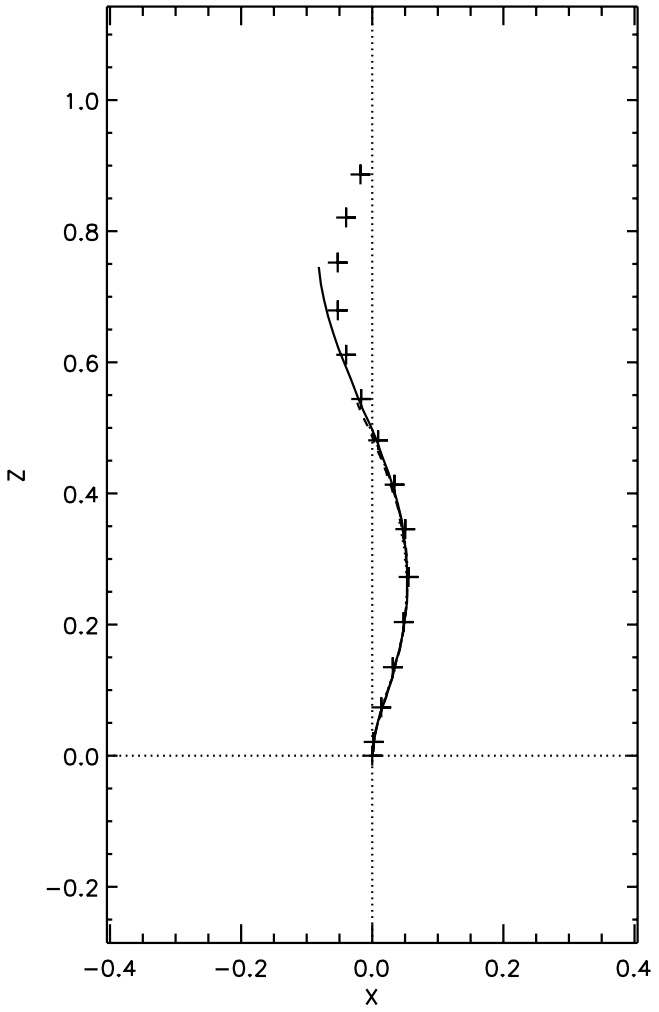

FIG. 3.—Trajectories of the center of the tube for buoyant magnetic tubes with $\beta = 50$ (*solid line*), $\beta = 100$ (*dot-dashed line*), $\beta = 200$ (*dashed line*), and $\beta = 400$ (*dotted line*). Time and length units are H_p/V_A and H_p, respectively. The four trajectories almost coincide. Plus signs represent the solution from eq. (6) that best fits the trajectory: $A = V_A^2(q^2H_p^2 + 4)/(16\gamma H_p)$, $\Omega = 0.6V_A/H_p \sin(1.18t + 0.465)$, $K = 18.2/H_p$, and $F = 2$. The deviation seen for $t > 10$ ($z > 0.6$) is caused by the tube expansion associated with the decrease in the external pressure.

$$F\frac{dv}{dt} = Ae_z - \Omega v \times e_y - K|v|v\,, \tag{6}$$

where F is the enhanced inertia factor, A is the global buoyancy acceleration of the tube, and the last term on the right-hand side is the mean drag exerted on the tube by the surrounding medium. The value of K cannot be determined except to within a factor of order unity. Following laboratory measurements, we take $K = C_D/(\pi R)$, with C_D the aerodynamic drag coefficient. It is of order unity for the range of Reynolds numbers used in this paper (see Emonet & Moreno-Insertis 1998). Equation (6) obviously can provide only a crude approximation to the actual motion of the tube. A major shortcoming is the fact that it does not account for the effect on the tube of the flows associated with the vortices as they move away from the wake. While it would not be difficult to reform the equation formally to account for the effect of external flows on a vortex filament, it would add a substantial complication to approximate the time-dependent velocity field associated with the moving external vortices. Such complication is unjustified in the present case; indeed, we show below that equation (6) accounts sufficiently well for the calculated trajectories within the limited accuracy required by the present test. Equation (6) is valid, strictly speaking, when all coefficients are constant.

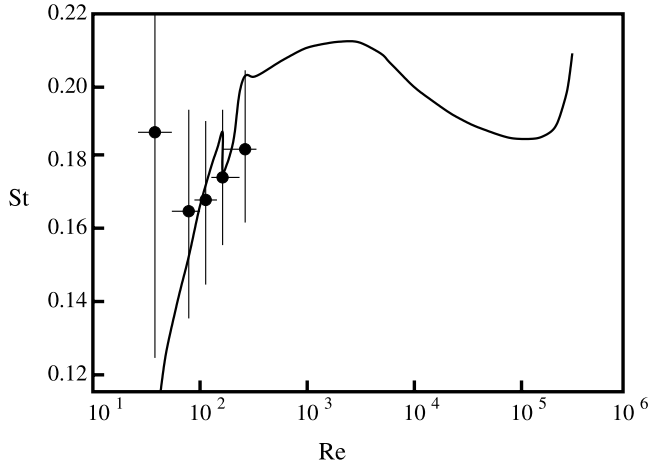

FIG. 4.—Frequency of vortex shedding (Strouhal number; *circles*) as a function of the Reynolds number for the five numerical experiments: $\beta = 50$ and μ, η, and κ changed by factors of 2. The solid line represents the hydrodynamic results on the Strouhal-Reynolds number relationship for vortex shedding of a circular cylinder (see Williamson 1988a, 1988b, 1996; Norberg 1994). Error bars correspond to the uncertainty in the determination of $D_{\rm tube}$, $V_{\rm tube}$, and Re. The large error bar for the point with the lowest value of Re is caused by the relatively large size of the boundary layer.

Equation (6) has different families of solutions depending on the values of the coefficients. The important dimensionless parameter is

$$\chi \equiv \frac{\Omega^2}{KA} = \frac{\tau_D^2}{\tau_\Omega^2}\,, \tag{7}$$

where $\tau_D = F/(KA)^{1/2}$ is the characteristic time necessary for the drag force to bring the velocity to its asymptotic regime and $\tau_\Omega = F/\Omega$ is the timescale over which the lift force modifies the speed of rise. For constant A, K, and Ω, the solutions can be understood as follows. In the *drag-dominated* regime ($\chi^2 \ll 1$), equation (6) yields a rectilinear trajectory that subtends an angle θ to the vertical given by

$$\cos\theta = -\frac{\chi}{2} + \sqrt{1 + \left(\frac{\chi}{2}\right)^2}\,, \tag{8}$$

along which the tubes move with speed

$$v^2 = (A/K)\cos\theta\,. \tag{9}$$

In the *drag-free* regime ($\chi^2 \gg 1$), equation (6) describes a horizontal drift of speed $v_{\rm drift} = A/\Omega$ combined with vertical oscillations of frequency $1/\tau_\Omega$ and amplitude FA/Ω^2. In the following two subsections, we discuss the application of these results to model the zigzag trajectories of rising flux tubes. First (§ 5.2), we discuss the drag-dominated case, which serves to explain the trajectories shown in § 3.2. In § 5.3, we study the trajectories obtained in $\chi > 1$ regimes.

5.2. *Drag-dominated Regime: Modeling the Zigzag Path*

An actual buoyant tube rising in a stratified medium does not have constant values of A, K, or Ω, but A and K are

nearly constant over the timescale τ_D on which the system described by equation (6) adapts to changes in those parameters. The integrated vorticity Ω varies in a cyclical fashion (roughly sinusoidally) on a timescale that, although shorter than that of A or K, is long compared with τ_D. Therefore, evaluating equations (8) and (9) with the instantaneous values of A, Ω, and K, we obtain approximate values for the vertical and horizontal components of the velocity vector along the trajectory as follows:

$$v_z = (A/K)^{1/2},\ v_x \approx \Omega/K\ . \tag{10}$$

Equation (10) predicts an upward trajectory with a superposed sinusoidal horizontal oscillation.[3]

We can now try to reproduce the simulated trajectories using the full equation (6). Analytical integration of the initial condition yields $A = V_A^2(q^2H_p^2 + 4)/(16\gamma H_p)$. From the numerical simulation, we obtain $K = 18.2/H_p$ and $F = 2$. Ω is difficult to obtain. We set it equal to a sinusoidal function with amplitude fixed by an optimum fitting to the experimental paths. This yields $\chi = 0.25$ for all the cases calculated in § 3.2. The resulting solution to equation (6) is overplotted in Figures 3 and 5 with plus signs.

The actual trajectory of the tube is remarkably well approximated by this solution: this suggests that equation (6) does indeed contain the essential ingredients that determine the zigzag path of the rising tube and that the trajectories are mainly sensitive to the parameter χ. Deviations in the upper third of the integration box are caused by the expansion of the tube following the rapid decrease in the external pressure, an effect not included in equation (6).

In the drag-dominated regime we thus have the result that neither χ nor the trajectories vary if we modify β keeping the Reynolds numbers fixed. In fact this is a direct consequence of the scaling law, equation (4). This can be seen as follows: The vorticity amplitude for any particular case is proportional to the product of vorticity generation rate ($\propto \mathrm{Re}_m^{1/2}/\beta$, eq. [4]) multiplied by the timescale ($\propto \beta^{1/2}$). Using $A \propto \beta^{-1}$ in (7), we immediately obtain $\chi \propto \mathrm{Re}_m$, with no direct dependence on β. The maximum horizontal elongation of the trajectory is, from equation (10), proportional to the amplitude of Ω divided by the frequency of vortex shedding. The latter two quantities are proportional to $\beta^{-1/2}$ and the result follows. In all the foregoing, we have used the fact that the drag coefficient K does not depend on β or Re_m (we assume that the drag is entirely aerodynamic, not too bad an approximation as long as $10^2 \leq \mathrm{Re} \leq 2 \times 10^5$; see Tritton 1977).

5.3. *The Trajectory of the Tube in the Drag-free and Intermediate Regimes* ($\chi > 1$)

As shown in the previous section, in the drag-dominated regime χ is directly proportional to the Reynolds number. Modifying the diffusivities so that Re_m and Re grow but leaving unchanged all other parameters of the problem causes two kinds of modifications in the trajectories: first, both the amplitude of the horizontal velocity and of the horizontal elongation of the trajectory increase (eq. [10]); second, the frequency of vortex shedding grows, although only very weakly, with Re (§ 4). If we continue raising the Reynolds numbers, χ will grow upward of 1 and the tube will enter an intermediate regime and, for still higher χ, the drag-free regime.

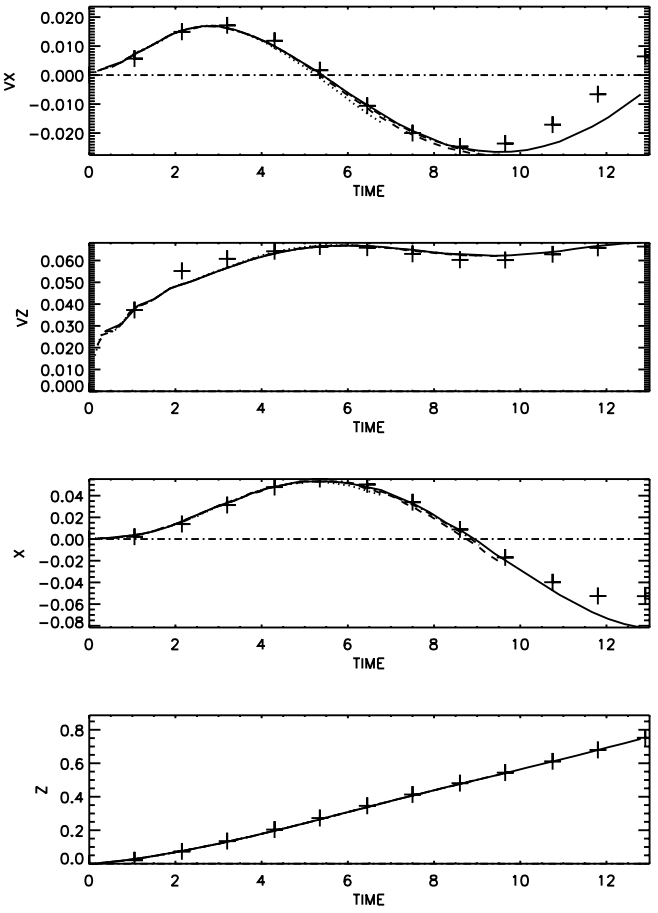

FIG. 5.—Time evolution of the horizontal and vertical velocities and positions of the center of the tube for the four cases of Fig. 3. Time and length units are H_p/V_A and H_p, respectively. As in Fig. 3, the four curves almost coincide. Plus signs represent the solution from eq. (6) that best fits the numerical result.

In the high-χ regime, some of the approximations made in this paper are no longer granted, such as the form of the drag term, the scaling laws of equations (4) and (5), possibly also the simple periodic shedding of vortices, etc. However, it may be instructive to see the kind of changes in the solutions of equation (6) as we let χ grow upward of 1. In Figure 6, we are showing the trajectories corresponding to the solutions for $\chi = 1$, 10, and 20 keeping for Ω the sinusoidal shape and dimensionless frequency used in the foregoing section. Note that the $\chi = 20$ trajectory may well be unrealistic since there is no guarantee that the simple sinusoidal shape for Ω is kept in this regime. As we see, while $\chi = 1$ still yields a trajectory very much like those in the drag-dominated regime, as soon as $\chi^2 \gg 1$ the trajectory shows one or more *epicycles* superposed on each of the horizontal oscillations. As χ grows, so do the number of epicycles on each lateral excursion of the tube: they increasingly resemble the purely inertial oscillations predicted by equation (6) for constant Ω and large χ. The trajectory thus has periods of mainly vertical buoyant rise with low lift force (when $|\Omega|$ is going through a node) separated by stretches of mostly horizontal motion with inertial oscillations superposed (when $|\Omega|$ is not far from its maximum amplitude). The

[3] Interestingly, it can be shown (T. Bogdan 1999, private communication) that, in the drag-dominated regime, the asymptotic trajectories to eq. (6) are stable to small perturbations. In the drag-free regime, a perturbation will induce a decaying oscillation on the trajectory.

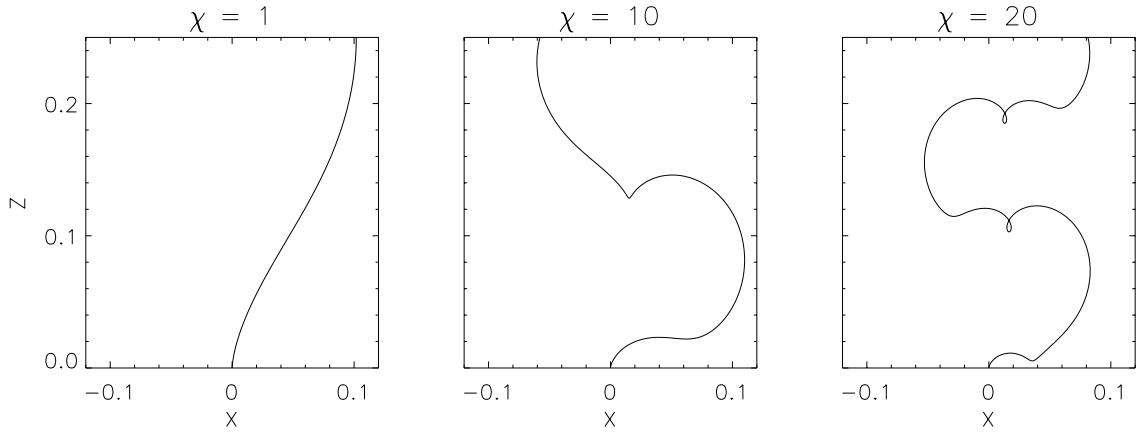

FIG. 6.—Trajectories calculated by integrating numerically eq. (6) for different values of χ (or Ω) and constant F, A, and K (for these we use the same values as for the plus signs in Figs. 3 and 5).

horizontal excursions cause a delay in the rise: that can be seen directly in Figure 6 from the fact that the right-left oscillation of the tube has the same frequency in all cases, whereas the successive vertical cuts of the trajectories with the central vertical axis are closer together the higher the value of χ. More precisely, we find the time necessary for the tube to reach a certain height to increase approximately as $\chi^{1/2}$.

It is not clear in how far the involved trajectories for the higher values of χ in Figure 6 will be realized in an actual experiment with a flux tube. However, at least the curves for the lower χ-values shown in the figure seem to have been reported in the literature, as we comment in the following section.

6. SUMMARY AND DISCUSSION

We have studied the generation of vorticity in the boundary layer surrounding a buoyant flux tube and how it affects the rise trajectory depending on the values of plasma beta and Reynolds numbers. The parameter ranges used here are 25 to 800 for β, 50 to 300 for Re, and 100 to 600 for Re_m.

The generation of vorticity is caused mainly by the magnetic stress. In a drag-dominated regime (i.e., with the drag force exactly matching the driving forces), the vorticity generation rate scales as $\mathrm{Re}_m^{1/2}/\beta$ (§ 2). The β^{-1} proportionality is confirmed by our numerical results (§ 3.1). We have modeled the rise of a tube with a wake that is unstable and leaves behind a von Kármán vortex street. The tube is thus surrounded by a flow with nonzero circulation for which the sign changes periodically in time. The ensuing oscillating lift force on the tube causes the rising trajectory to be sinusoidal instead of just rectilinear. Still, if the conditions of drag domination and fixed Reynolds numbers below 1000 apply, all forces in the equation of motion of those tubes also follow a scaling β^{-1}. Since the timescale of the rise is proportional to $\beta^{1/2}$, the equation of motion yields a trajectory that is independent of β.

If we maintain β constant, then for increasing values of the Reynolds numbers we find (§ 4) that the dimensionless frequency of vortex shedding (the Strouhal number, St) off the magnetic tube in our simulations is close to the Strouhal-Reynolds number relationship for vortex shedding of a circular cylinder found in the hydrodynamic literature (the discrepancy is less than 20%). Unlike the changes in β, the increase in the Reynolds numbers produces a change in the trajectory, which becomes more involved. These modifications of the trajectory can be explained using a simple analytical model: We have shown in § 5 that an equation of motion including buoyancy force, drag, and the lift adequate to a vortex filament (eq. [6]) can well approximate the rising zigzag path of the tube. The important dimensionless parameter in that equation, χ, is the square of the ratio between the characteristic timescale of the drag (τ_D in § 5.1) and the period of the inertial oscillations associated with the lift force (τ_Ω). The parameter χ is found to be independent of β (for β well above 1) and proportional to Re. The drag-dominated regime can be expected whenever $\chi^2 \ll 1$. The results of §§ 2 and 3 have been obtained for tubes that fulfill that condition.

Raising Re and Re_m beyond, say, 500 *while holding* β *constant* leads to increased vorticity production for the same buoyancy and drag coefficient K. Thus, the parameter χ increases and eventually becomes larger than 1. The solutions to equation (6) in this dynamically very different domain still show a trajectory oscillating from left to right around the vertical, but now the horizontal excursions contain epicyclic episodes (§ 5.3). The number of the epicycles and the duration of the horizontal excursions grows with increasing χ.

As explained in § 5.3, when $\chi^2 \gg 1$ (drag-free regime) the approximations made in this paper are no longer granted: the form of the drag term and the assumption of a periodic shedding become inaccurate. Yet, our analysis may still account for the behavior of magnetic tubes with χ not far above 1, i.e., in an intermediate regime between drag dominated and drag free. In fact, comparison between our Figure 6 and the trajectories found by Hughes & Falle (1998; see Figs. 3 and 4 in their paper) seems to indicate that the complicated behavior of their tube when the Reynolds number is high ($\mathrm{Re} \simeq 4000$) can be explained with our simple analytical model. Using grid-refinement methods, those authors present trajectories for two tubes with the Reynolds number differing by a factor of 16 while holding $\beta = 10$ for both. The curve for the higher Reynolds number shows a quasi-epicyclic episode not unlike case $\chi = 10$ of our Figure 6. Lower β-values, however, render a comparison with the scaling laws of equations (4) and (5) difficult since the lower order terms of equation (1) may cease to be

negligible (at any rate, the magnetic tubes in the convection zone have β of order 10^5 or higher).

The range of Reynolds numbers accessible to numerical calculations with the currently available computer power is very limited in comparison with what would be needed to properly simulate astrophysical fluids. The problem is not so severe for the plasma beta parameter, which, in stellar interiors, is probably just a factor of 10 to 100 larger than values within computational reach. In contrast, Re and Re_m for, e.g., buoyant magnetic tubes of total magnetic flux 10^{22} Mx at the bottom of the convection zone, are off by *several* orders of magnitude from the values that can be dealt with by today's computers and codes. Hints for the behavior in higher Reynolds number ranges must come, therefore, first from more expensive simulations with adaptive refinement techniques and then, for Reynolds numbers closer to the stellar ones, from the hydrodynamic literature of experiments on flows around rigid cylinders.

The instabilities appearing in very high Reynolds number flows (turbulence, three-dimensional wake instabilities, etc.) change the flow structure around the tube from the relatively simple cases seen in the numerical simulations and may thus also alter the total amount of vorticity around the tube to an unknown extent. However, even when the Reynolds number becomes fairly high, $O(2 \times 10^5)$, attached recirculation regions and vortex shedding are still observed in the wake of rigid cylinders in water (Williamson 1996). This indicates that the process of vortex shedding and its effect on the trajectory of the tubes is likely to be an important ingredient of the dynamics of at least some of the magnetic structures moving through the solar convection zone.

We are grateful to T. Bogdan for his careful reading of a draft of this paper and for making a stability analysis of the analytical solutions presented in § 5. This work was supported through DGESIC project C95-0028C (Spanish Ministry of Education and Culture). The computations have been supported in part by NASA Cooperative Agreement Notice NCCS5-151. The National Center for Atmospheric Research is sponsored by the National Science Foundation.

REFERENCES

Berger, E., & Wille, R. 1972, Annu. Rev. Fluid Mech., 4, 313
Emonet, T., & Moreno-Insertis, F. 1998, ApJ, 492, 804
Fan, Y., Zweibel, E. G., & Lantz, S. R. 1998a, ApJ, 493, 480
Fan, Y., Zweibel, E. G., Linton, M. G., & Fisher, G. H. 1998b, ApJ, 505, L59
Hughes, D. W., & Falle, S. A. E. G. 1998, ApJ, 509, L57
Moreno-Insertis, F. 1997a, in Solar Magnetic Fields, ed. V. H. Hansteen (Oslo: Univ. Oslo), 3
———. 1997b, Mem. Soc. Astron. Italiana, 68, 429
Moreno-Insertis, F., & Emonet, T. 1996, ApJ, 472, L53
Norberg, C. 1994, J. Fluid Mech., 258, 287
Parker, E. N. 1982, Sol. Phys., 77, 3
Rast, M. P. 1998, J. Fluid Mech., 369, 125
Saffman, P. G. 1992, Vortex Dynamics (Cambridge: Cambridge Univ. Press)
Szepessy, S., & Bearman, P. W. 1992, J. Fluid Mech., 234, 191
Tritton, D. J. 1977, Physical Fluid Dynamics (Oxford: Oxford Univ. Press)
Williamson, C. H. K. 1988a, Phys. Fluids, 31, 2742
———. 1988b, Phys. Fluids, 31, 3165
———. 1996, Annu. Rev. Fluid Mech., 28, 477